Journal of
Biomedical Optics

SPIEDigitalLibrary.org/jbo

Photoacoustic lifetime contrast between methylene blue monomers and self-quenched dimers as a model for dual-labeled activatable probes

Ekaterina Morgounova
Qi Shao
Benjamin J. Hackel
David D. Thomas
Shai Ashkenazi

SPIE

Journal of Biomedical Optics 18(5), 056004 (May 2013)

Photoacoustic lifetime contrast between methylene blue monomers and self-quenched dimers as a model for dual-labeled activatable probes

Ekaterina Morgounova,[a] Qi Shao,[a] Benjamin J. Hackel,[b] David D. Thomas,[c] and Shai Ashkenazi[a]
[a]University of Minnesota, Department of Biomedical Engineering, 312 Church Street SE, Minneapolis, Minnesota 55455
[b]University of Minnesota, Department of Chemical Engineering and Materials Science, 421 Washington Ave. SE, Minneapolis, Minnesota 55455
[c]University of Minnesota, Department of Biochemistry, Molecular Biology and Biophysics, 321 Church Street SE, Minneapolis, Minnesota 55455

Abstract. Activatable photoacoustic probes efficiently combine the high spatial resolution and penetration depth of ultrasound with the high optical contrast and versatility of molecular imaging agents. Our approach is based on photoacoustic probing of the excited-state lifetime of methylene blue (MB), a fluorophore widely used in clinical therapeutic and diagnostic applications. Upon aggregation, static quenching between the bound molecules dramatically shortens their lifetime by three orders of magnitude. We present preliminary results demonstrating the ability of photoacoustic imaging to probe the lifetime contrast between monomers and dimers with high sensitivity in cylindrical phantoms. Gradual dimerization enhancement, driven by the addition of increasing concentrations of sodium sulfate to a MB solution, showed that lifetime-based photoacoustic probing decreases linearly with monomer concentration. Similarly, the addition of 4 mM sodium dodecyl sulfate, a concentration that amplifies MB aggregation and reduces the monomer concentration by more than 20-fold, led to a signal decrease of more than 20 dB compared to a solution free of surfactant. These results suggest that photoacoustic imaging can be used to selectively detect the presence of monomers. We conclude by discussing the implementation of the monomer–dimer contrast mechanism for the development of an enzyme-specific activatable probe. [DOI: 10.1117/1.JBO.18.5.056004]

Keywords: photoacoustic imaging; activatable probes; methylene blue; static quenching; excited-state lifetime; photoinduced electron transfer.

Paper 12767R received Dec. 2, 2012; revised manuscript received Mar. 19, 2013; accepted for publication Mar. 26, 2013; published online May 2, 2013.

1 Introduction

Photoacoustic molecular imaging is a nonionizing modality that provides high penetration depth and high spatial resolution information on the functional and metabolic status of diseases at greater depths than other optical imaging techniques.[1–3] Traditionally, photoacoustic imaging has been used with both endogenous contrast agents, such as hemoglobin and melanin, and exogenous contrast agents that exhibit higher optical absorption than normal tissue. Targeting molecular markers using exogenous smart probes can potentially reap valuable information about biological processes occurring at different stages of various diseases. As a result, photoacoustic molecular imaging could substantially aid the diagnosis of cancer by detecting subtle abnormalities at the molecular level well before the appearance of anatomical changes.[4] This capability would also allow for personalized treatment planning and step-by-step evaluation of treatment efficacy.[2]

Our research focuses on the development of a new photoacoustic contrast agent based on the lifetime sensing of methylene blue (MB) dye. MB monomers present a high quantum yield of intersystem crossing ($\Phi_{\mathrm{ISC}} > 0.50$)[5] and a long triplet excited-state lifetime ($\tau > 70\ \mu\mathrm{s}$).[6] Upon aggregation, static quenching between strongly bonded molecules dramatically shortens their excited-state lifetime by 2 to 3 orders of magnitude.[7] This forms the basis of a highly sensitive contrast mechanism between MB monomers and dimers. A promising application is the development of a MB-labeled smart probe activated by enzymatic cleavage. The probe's signal is highly suppressed in the bound state, however, it recovers its long excited-state lifetime after activation which is then detectable by photoacoustic lifetime contrast imaging (PLCI) (Fig. 1).

1.1 *Activatable Probes for Molecular Imaging*

Activatable probes are a class of contrast agents that identify selective enzyme activity by switching from an inactive state to an active state upon interaction with a target enzyme.[8] Originally developed for fluorescence imaging, the probes contained a fluorophore-quencher pair coupled to a peptide linker bearing an enzymatic site.[9] Upon cleavage of the linker, the pair is separated and fluorescence is restored. This approach provides high contrast because of the low fluorescence background of the uncleaved, inactive form. Additionally, the fluorescence signal is further amplified due to the activation of multiple probes by a single enzyme.[10]

Activatable fluorescent probes have been successfully used in a wide range of small-animal imaging studies. However, the short penetration depth of light in tissue resulting from strong optical attenuation and scattering limits their translation to

---

Address all correspondence to: Ekaterina Morgounova, University of Minnesota, Department of Biomedical Engineering, 312 Church Street SE, Minneapolis, Minnesota 55455. Tel: 612-625-1833; Fax: 612-626-6583; E-mail: emorgoun@umn.edu

0091-3286/2013/$25.00 © 2013 SPIE

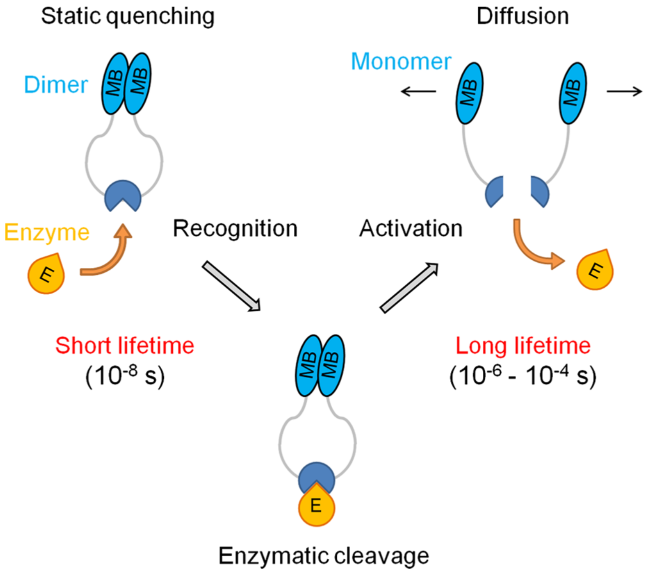

Fig. 1 Schematic representation of proposed MB dual-labeled activatable probe containing a specific enzymatic site. The intact probe has a short lifetime of a few tens of nanoseconds. Enzymatic cleavage separates the chromophores thereby permitting them to recover their long excited-state lifetime (tens of microseconds).

clinical applications and leads to poor spatial resolution beyond a few millimeters.[11] Photoacoustic imaging has emerged, in the last two decades, as an alternative optical modality offering significantly improved resolution (up to 0.02 mm) and penetration depth (up to 5 cm) in tissue imaging.[1] Its application has been demonstrated in clinical studies for breast cancer screening[12] and skin cancer diagnosis.[13]

Activatable photoacoustic probes have recently been proposed and studied by several groups.[2,3] They rely on a change in the absorption spectrum upon activation to selectively detect the activated probe signal. This method requires multiwavelength illumination to resolve the spectral contribution of each chromophore by linear fitting and also assumes that the spectral distribution of probes and tissue absorbers is known. In practice, nonuniform light distribution, due to wavelength-dependent attenuation, and heterogeneous optical properties of tissue may hamper accurate spectral identification and background signal suppression.

In this work, we propose a new photoacoustic contrast mechanism that is based on switching the excited-state lifetime of the probe from short (<100 ns) to long (>2 μs). PLCI, a pump-probe approach that eliminates the need for spectral deconvolution by measuring lifetime contrast using only two illumination wavelengths, is applied for the first time to selectively detect the signal from activated probes.

1.2 *Photoacoustic Lifetime Contrast Imaging*

MB is a planar cationic dye of the phenothiazine family with an absorption peak at 664 nm in its monomer form (Fig. 2). It is commonly used, or under study, in several therapeutic and diagnostic applications.[14,15] Both orally and intravenously administered MB is excreted by the kidneys either unchanged or reduced to leucomethylene blue by the enzyme methemoglobin reductase present in red blood cells.[16,17] Following optical absorption, the ground state molecule (S_0) is excited into a singlet state (S_1), and then undergoes intersystem crossing (ISC) to a metastable triplet state (T_1) with high quantum yield ($\Phi_{\mathrm{ISC}} = 0.50$)[5] (Fig. 3). The excited triplet state lifetime is typically tens of microseconds in an oxygen-free environment because of the spin-forbidden nature of the $T_1 - S_0$ transition. Collisional quenching by oxygen, however, decreases this lifetime to approximately 2 μs in aerated solutions at atmospheric pressure.[18]

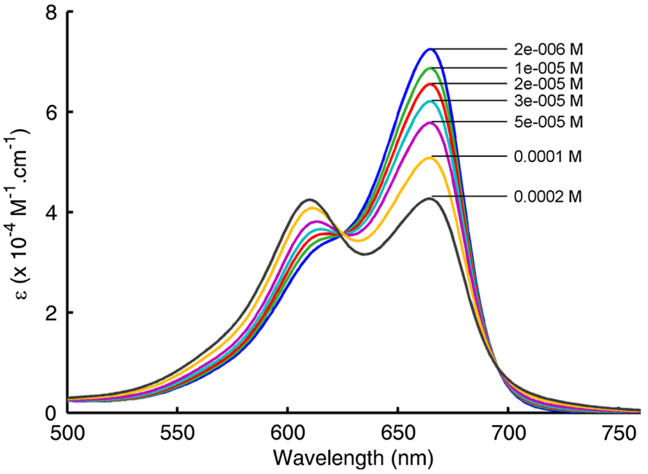

Fig. 2 Absorption spectra of MB in water (2 to 200 μM). The absorption maximum shifts from 665 to 608 nm with increasing [MB] indicating an increase in the dimer-to-monomer molar ratio. The isosbestic point at 625 nm is shifted towards the blue wavelengths for [MB] >100 μM due to the formation of higher order aggregates.

Molecular association between monomers occurs spontaneously in water due to a combination of hydrophobic interactions,

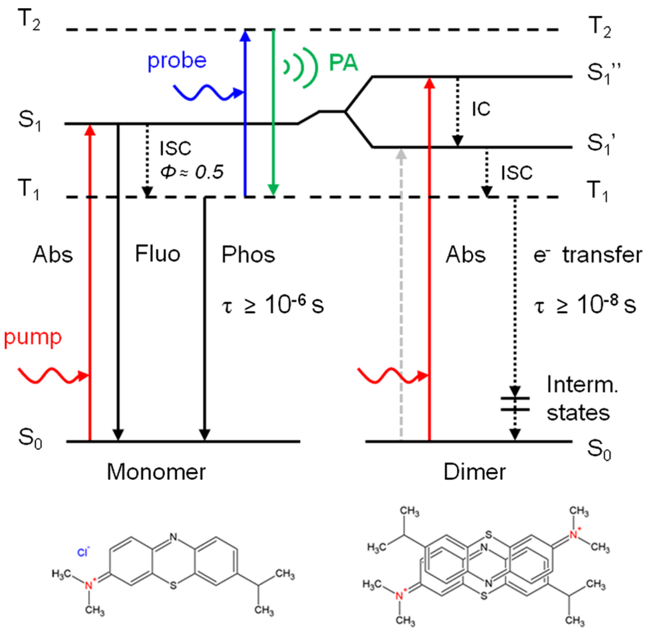

Fig. 3 Energy diagram of MB monomer and dimer. Plain lines represent radiative transitions. Small downward dashed lines represent nonradiative processes. The energy of the $T_1:T_2$ absorption is converted into a photoacoustic relaxation signal. The double bar indicates a discontinuity in the transition diagram: the dimer triplet undergoes electron transfer (~40 ns) which leads to the formation of oppositely charged radicals that relax to the ground state via charge recombination (~10^{-6} to 10^{-4} s). S_0: ground state, S_1: singlet excited state, T_1: primary triplet excited state, T_1: secondary triplet excited state, S_1' and S_1'': split exciton states, ISC: intersystem crossing, IC: internal conversion. Bottom: possible configurations of MB monomer and H-type dimer.

hydrogen bonding, and Van der Waals forces.[19,20] The coupling between monomers results in a splitting of the singlet excited state into two states, of lower and upper energies, which manifests by a splitting of the absorption band of the monomer (Fig. 3).[19,21–23] Figure 2 shows a shift in the absorption peak from 665 to 608 nm with increasing MB concentrations. This corresponds to the preferential transition to a higher energy state which results in a dominant blue-shifted peak specific of H-type (or face-to-face) dimers. If a dimer is excited to the upper state S_1, it undergoes very fast (10^{-12} s) internal conversion to the lower state S_1' and, because transitions from S_1' to S_0 are forbidden, ISC is enhanced. If the coupling between monomers is strong, electron transfer is expected to occur between the pair which results in triplet lifetime quenching and formation of transient radical ion pairs.[24,25] Excitation of an aqueous MB solution revealed the existence of a fast transient derived from the dimer, allegedly a triplet state, which decays into a slow transient pair formulated as a charge-transfer.[26] In an experiment mixing MB with sodium dodecyl sulfate (SDS), a compound that promotes MB dimerization at specific concentrations, Junqueira et al. reported lifetimes of 40 ns, 1.6 and 300 μs for the triplet, radical anion and radical cation, respectively.[27]

PLCI is a pump-probe approach that consists of applying an initial laser pulse (pump) to excite the dye to the T_1 state and a secondary pulse (probe) to excite T_1 to a T_2 state resulting in ultrasound waves generated during the $T_2 \rightarrow T_1$ photoacoustic relaxation (Fig. 3). With this technique, the amplitude of the measured photoacoustic signal corresponds to the sum of the lifetime-dependent photoacoustic relaxation, a quantity proportional to the optical absorption of the T_1 state, and the lifetime-independent background photoacoustic signal due to the excitation of the background environment by the probe pulse. By repeating a sequence of pulse pairs with different time delays between pump (dye excitation) and probe (photoacoustic wave generation) pulses, we can measure the decay dynamics of the triplet state and extract the excitation lifetime by exponential fitting. This technique has been recently demonstrated for quantitative measurement of dissolved oxygen levels in phantom objects by our research group.[18]

There exists a distinct separation of lifetimes between MB monomers, MB dimers, and main biological components, such as hemoglobin, albumin and melanin,[28–31] that can be exploited to efficiently suppress all photoacoustic signals arising from absorbers having lifetimes shorter than a set threshold. Figure 4 shows the normalized photoacoustic signal of hemoglobin, MB dimers, and MB monomers in low oxygen environment measured after probe excitation in a uniformly illuminated sample. Since MB monomers and dimers do not absorb at the probe wavelength (800 to 850 nm),[32] the background photoacoustic signal is constant and equal to the value after complete relaxation of the chromophores, i.e., $\mathrm{PA}_{100\,\mu s}$. It can be seen that, by subtracting two photoacoustic signals taken with a pump-probe delay of 1 and 100 μs, the only contribution comes from monomers. Additionally, dividing the difference signal by $\mathrm{PA}_{100\,\mu s}$ normalizes the monomer signal to the probe laser energy which corrects for energy deposition fluctuations within the illuminated sample. A photoacoustic contrast parameter, as defined in Eq. (1), is proportional to the monomer concentration:

$$C_{\mathrm{PLCI}} = \frac{\mathrm{PA}_{1\,\mu s} - \mathrm{PA}_{100\,\mu s}}{\mathrm{PA}_{100\,\mu s}} = \frac{\mathrm{PA}_{\mathrm{monomer}}}{\mathrm{PA}_{\mathrm{background}}} \propto [\mathrm{monomer}]. \quad (1)$$

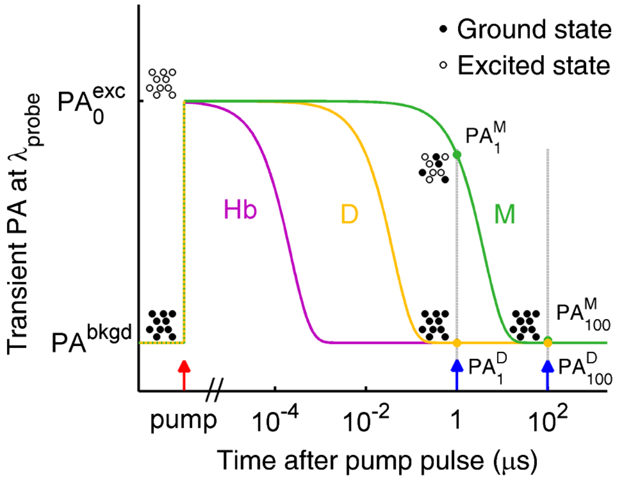

Fig. 4 Normalized transient photoacoustic signal for MB monomer ($\tau = 4\ \mu$s), dimer ($\tau = 40$ ns), and hemoglobin ($\tau = 0.22$ ns).

1.3 *Study Goal*

The goal of this study was to investigate two dimerization models to validate the contrast mechanism between MB monomers (activated probes) and dimers (inactive probes). The first system involves sodium-sulfate-driven dimerization caused by the increase of hydrophobic interactions with ionic strength. The second system incorporates dimerization induced by SDS premicellar aggregates. We have used these two systems to switch between high dimer concentration and high monomer concentration and to demonstrate that PLCI can achieve an efficient suppression of the dimer signal relative to that of the monomer.

2 Materials and Methods

2.1 *Materials*

Methylene Blue hydrate (purum ≥ 97%), and SDS (≥ 99.0%) were acquired from Sigma-Aldrich (St. Louis, Missouri) and sodium sulfate anhydrous (ACS) was acquired from Mallinckrodt Chemicals (Phillipsburg, New Jersey). All chemicals were dissolved without further purification in distilled water. Absorption and flash-photolysis measurements involving SDS were completed within 3 min after MB dilution. Experiments were performed at 22 ± 1°C, and the pH of the solutions was measured to be within 6.7 ± 0.9. Changes in temperature and pH level, in these ranges, do not have a significant effect on MB dimerization.

2.2 *Absorption Measurements*

Absorption spectra were recorded on a UV/Vis CaryUV Varian spectrophotometer using glass and plastic cuvettes of 0.1, 0.5 and 1 cm thickness. Triplet transient absorption was measured, independently from PA experiments, at fixed wavelengths by laser flash photolysis. The pump pulses were generated by an optical parametric oscillator (OPO, Opotek MagicPrism, Califonia) pumped by a tripled Nd:YAG pulsed laser (Surelite I-10, Continuum, Califonia, $f = 10$ Hz, pulse width = 5 ns). The solution-filled cuvettes were probed by a laser diode ($\lambda = 808$ nm, $P = 150$ mW) emitting continuously at a right angle with respect to the pump laser beam. The probe beam, once transmitted through the sample, is bandpass filtered (FB810-10, Thorlabs, Pennsylvania, central frequency = 810 nm) and measured by a Si photodetector (DET10A, Thorlabs, Pennsylvania). The signal is recorded by a digital oscilloscope (Lecroy, Wavejet 354) and transferred to a computer for processing. All the experimental data were processed and analyzed with MATLAB.

2.3 *Photoacoustic Experimental Setup*

A PLCI experimental setup was used to probe the photoacoustic signal of plastic tubes filled with dye, mixed salt/dye, or SDS/dye solutions as illustrated in Fig. 5. Two tunable Nd:YAG pulsed-laser systems (Surelite I-10, Continuum and Quantel, Brilliant both having $f = 10$ Hz, pulse width $= 5$ ns), each coupled to an OPO (Opotek MagicPrism, Califonia), delivered the pump and probe pulses (6 and 8 mJ, respectively). The output of both OPO systems was coupled to a bifurcated light guide (Dolan-Jenner, EE436, nonrandomized for salt experiment or Moritex, MWG-1000S-SD, randomized for SDS experiment) to ensure uniform illumination of the plastic tubes. The tubes were immersed in a water tank and a focused ultrasound transducer (Panametrics, V382, 3.5 MHz for salt experiment or V311, 10 MHz for SDS experiment) aligned with the incident laser beams detected the photoacoustic signals generated in the samples. Laser firing and ultrasound acquisition were synchronized by a field-programmable gate array (FPGA, KNJN, FX2 Saxo). Signals were amplified by 50 dB (Panametrics, 5072PR), recorded by a digital oscilloscope (Lecroy Wavejet 354), and transferred to a computer for processing. B-mode images were acquired by scanning the tubes, perpendicular to their long axis, using a motorized actuator (T-LA28A, Zaber) mounted on a translation stage. In order to maximize contrast, the wavelengths of both beams were independently tuned near the maximum of absorption for the monomer and triplet species, and within the range of maximal output energy for the OPOs.

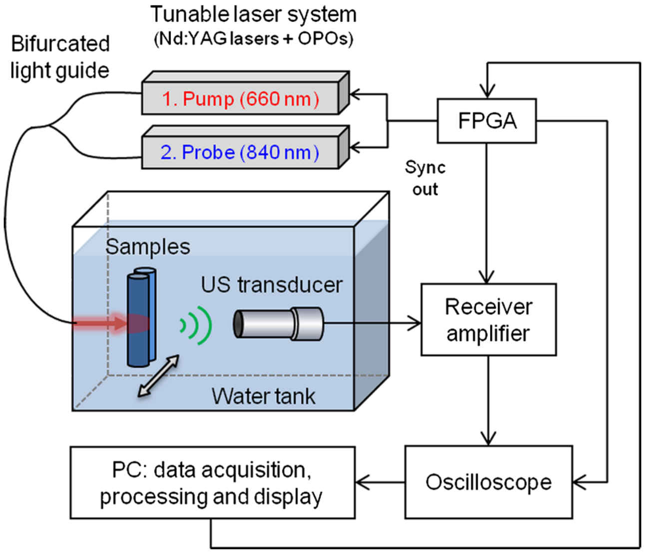

Fig. 5 PLCI experimental setup. Pulsed outputs of the excitation laser (660 nm) and photoacoustic laser (840 nm) were combined with a bifurcated light guide and illuminate the target. The time delay between the excitation and probe pulses was controlled by an electronic synchronization circuit. The solutions were placed in two plastic tubes and scanned horizontally. The generated acoustic waves were detected by a focused ultrasound transducer. *Sync out:* synchronization output.

2.4 *Calculation of Monomer and Dimer Concentrations*

The individual monomer and dimer spectra were obtained using a two-state model analysis of the spectral data in the concentration region where the monomer–dimer equilibrium is dominant (2 to 50 μM), as indicated by a stable isosbestic point at 625 nm (Fig. 2). For concentrations greater than 50 μM, we observed a progressive blue shift of the isosbestic point that can be attributed to the formation of a small amount of trimers (with absorption maximum at 580 nm).[33] In this model (adapted from Patil et al.[20]), the dimer dissociation constant K_D is defined as Eq. (2):

$$K_D = \frac{[M]^2}{[D]} = \frac{2x_M^2 C}{(1 - x_M)}, \tag{2}$$

where C is the total concentration of the dye, $C = [M] + 2[D]$, and x_M is the monomer molar fraction, $x_M = [M]/C$. If we assume that we have only two species in solution, then the Beer–Lambert law is applicable to those species as depicted in Eq. (3):

$$A^\lambda = \varepsilon^\lambda \cdot l \cdot C, \tag{3}$$

where the observable molar absorption coefficient ε^λ can be expressed as a function of the individual molar absorption coefficient of the monomer ε_M^λ and the dimer $\frac{\varepsilon_D^\lambda}{2}$ Eq. (4):

$$\varepsilon^\lambda = x_M \varepsilon_M^\lambda + (1 - x_M)\varepsilon_D^\lambda/2, \tag{4}$$

also written in the linear form as depicted in Eq. (5):

$$\varepsilon^\lambda = x_M * (\varepsilon_M^\lambda - \varepsilon_D^\lambda/2) + \varepsilon_D^\lambda/2. \tag{5}$$

We computed a linear regression to model the relationship between the molar absorption coefficient ε^λ, measured for different concentrations, and the monomer molar fraction at those concentrations in order to calculate the value of the dissociation constant K_D that minimizes the sum-of-squared residuals over several wavelengths. We found a K_D value of 2.6×10^{-4} M which is in good agreement with the value reported by Patil et al.[20] (2.9×10^{-4} M, at 27°C) and by Rabinowitch and Epstein[34] (2.8×10^{-4} M, at 26.7°C).

The ε_M and $\varepsilon_D/2$ values, at different wavelengths, were extracted from the slope and origin of the linear fit and used to generate the individual monomer and dimer spectra [dashed lines in Fig. 6(a)]. Assuming that we have a two-component system, we can use a rearranged form of Eq. (4) to establish a concentration-independent relationship between the dimer-to-monomer absorption peak ratio and the true monomer molar fraction, as shown in Eq. (6):

$$x_M = f\left(R = \frac{\varepsilon_D^{\lambda_D^{\max}}}{\varepsilon_M^{\lambda_M^{\max}}}\right) = \frac{\varepsilon_D^{\lambda_D^{\max}}/2 - R * \varepsilon_D^{\lambda_M^{\max}}/2}{R * (\varepsilon_M^{\lambda_M^{\max}} - \varepsilon_D^{\lambda_M^{\max}}/2) - (\varepsilon_M^{\lambda_D^{\max}} - \varepsilon_D^{\lambda_D^{\max}}/2)}. \tag{6}$$

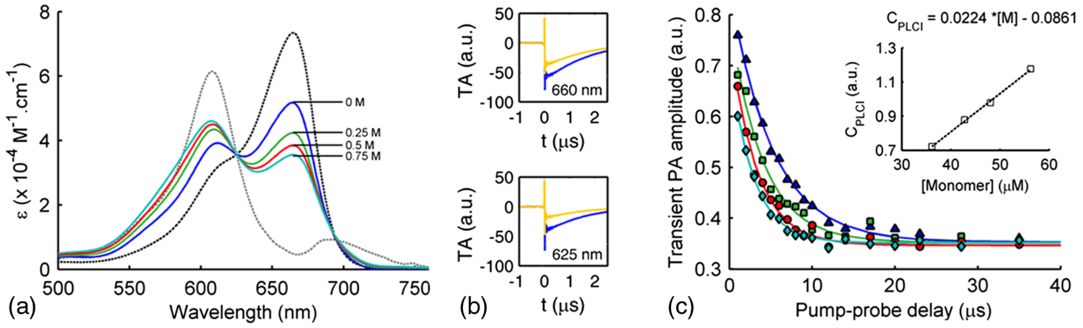

Fig. 6 (a) Solid lines: absorption spectrum of a solution of MB 80 μM for four different salt concentrations. Dashed lines: individual MB monomer (black) and dimer (gray) spectra in water. (b) Transient absorption (TA) of a solution of MB 80 μM with (orange/gray) and without Na_2SO_4 0.8 M (blue/black) measured by flash photolysis. Top: $\lambda_{exc} = 660$ nm. Bottom: $\lambda_{exc} = 625$ nm. (c) Transient photoacoustic signal amplitude as a function of pump-probe delay time acquired at four different Na_2SO_4 concentrations, 0 M (Δ), 0.25 M (□), 0.5 M (○), and 0.75 M (◇). Inset: the photoacoustic contrast parameter was observed to be linearly dependent on the estimated monomer concentration ($R^2 = 0.9980$).

3 Results and Discussion

3.1 *Dimerization in Sodium Sulfate*

MB dimerization can be enhanced by increasing the ionic strength of the solution which can be accomplished by adding salts such as sodium sulfate.[35] Figure 6(a) represents the absorption spectra of MB 80 μM, for increasing Na_2SO_4 concentrations, along with the individual monomer and dimer spectra calculated by applying a two-state model analysis to the data obtained in water. The spectra have been normalized to the isosbestic point in order to compensate for small concentration variations due to dilution uncertainty and a correction factor was calculated. The blue shift of the absorption maximum, from 665 to 608 nm, indicates that dimerization is enhanced with increasing salt concentration. The dimer peak does not exhibit a significant blue shift compared to the sole dimer spectrum (<1 nm for $[Na_2SO_4] = 0.75$ M), therefore, we conclude that trimerization does not significantly perturb the monomer–dimer equilibrium and we adopt the two-state model for the evaluation of the monomer fraction in each case.

We measured the triplet transient absorption of a solution of MB 80 μM, with and without Na_2SO_4 0.8 M, using flash-photolysis for $\lambda_{exc} = 660$ nm [Fig. 6(b), top] and observed that the amplitude of the signal decreases with the addition of salt while the lifetime remains unchanged. To ensure that this decrease is not due to a difference in absorption at the excitation wavelength, the experiment was repeated for $\lambda_{exc} = 625$ nm [Fig. 6(b), bottom] and yielded the same qualitative results. This indicates that MB dimers are statically quenched and that their triplet excited-state lifetime is short.

Finally, photoacoustic probing of the MB/salt solutions was performed in a single tube. MB monomers were excited at 660 nm and the triplet decay was probed at 800 nm for increasing pump-probe delay times. Figure 6(c) shows that the amplitude of the photoacoustic signal decreases with the salt concentration which is in agreement with the flash-photolysis results. The photoacoustic contrast parameter was calculated, between 1 and 100 μs, and plotted against the estimated monomer concentration [inset, Fig. 6(c)] which was obtained by multiplying the monomer molar fraction by the total MB concentration adjusted by the correction factor found from the absorption spectra. C_{PLCI} at the plastic-wall interface is in linear relationship with the monomer concentration ($R^2 = 0.9980$). We believe that the nonzero origin may be explained by an overestimation of the monomer concentration or a difference in local light distribution between 1 and 100 μs.

3.2 *Dimerization in Sodium Dodecyl Sulfate*

Despite their ability to increase dimer formation, salts have a limited power to overcome strong repulsive forces between MB molecules and do not induce full dimerization even at concentrations close to the solubility limit. SDS, on the contrary, is an anionic surfactant that binds MB due its opposite charge and provides a hydrophobic microenvironment that promotes dye aggregation on a larger scale. SDS concentrations as low as 1 mM have been shown to significantly increase MB dimerization.[7,27,36] The following experiments were realized within 3 min after MB dilution to ensure that the solutions remained stable over time.

Absorption measurements [Fig. 7(a)] revealed that the progressive addition of SDS to a 100 μM MB solution shifts the absorption maximum from 665 to 595 nm, thereby revealing the formation of H-type dimers ($\lambda_{max} = 608$ nm) and even higher order aggregates with lower absorption maxima. This is paralleled by a decrease in the triplet transient absorption measured by flash photolysis for $\lambda_{exc} = 660$ nm [Fig. 7(c)]. A maximum of polymerization occurs for [SDS] $\approx$ 4 mM [Fig. 7(b)] which corresponds to a minimum and a 25-fold decrease in the triplet transient absorption signal [Fig. 7(c)]. The same experiment conducted for $\lambda_{exc} = 600$ nm, a wavelength for which the extinction coefficient of dimers is twice the extinction coefficient of monomers, led to the same trend and a maximum of polymerization at 4 mM as well. Finally, we observed that the maximum of polymerization is invariant with respect to MB concentration by repeating the experiment for MB = 40 μM and for MB = 200 μM.

Junqueira et al. showed that the presence of increasing amounts of MB in SDS solutions decreases the critical micelle concentration (CMC) below the known CMC in water (7 to 8 mM).[26] Carroll et al. demonstrated that the scattering signal from a 1 μM MB solution exhibits a strong signal for [SDS] = 1.5 to 4.5 mM, suggesting the presence of a large aggregate in that range.[36] Those results indicate the formation of MB–SDS clusters or premicellar aggregates before the CMC is reached. We suggest that these premicelles are formed by strong electrostatic interactions between anionic SDS and cationic MB with the surfactant possibly intercalating its hydrophobic tail between adjacent MB molecules [Fig. 7(d)]. Water molecules might also

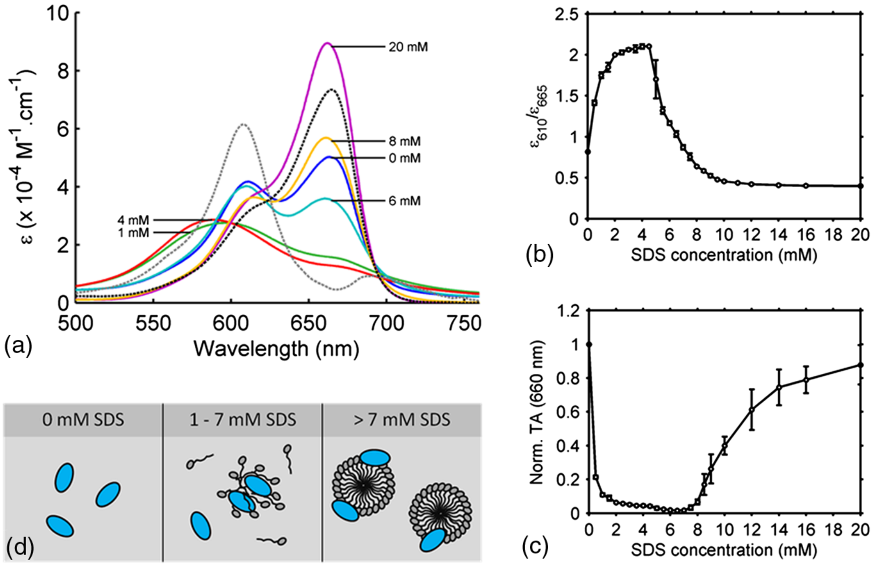

Fig. 7 (a) Solid lines: absorption spectrum of a solution of MB 100 μM ($x_M = 0.65$) for six different SDS concentrations. Dashed lines: individual MB monomer (black) and dimer (gray) spectra in water. (b) Dimer-to-monomer absorption peak ratio versus SDS concentration. (c) Triplet transient absorption measured at $t = 0^+$ after excitation (660 nm) versus SDS concentration. (d) Schematic representation of MB/SDS interactions at different SDS concentrations. The data points in (b) and (c) were obtained by averaging three independent measurements and normalizing to the signal measured in the absence of SDS.

help stabilize the MB/SDS complex by forming a hydrogen-bonded, shell-like structure called an "iceberg structure."[37] The distance between MB molecules, inside the premicelles, are short (corresponding to high local concentration) which promotes dimer formation.

At intermediate surfactant concentrations ($4.5 < [\mathrm{SDS}] < 7$ mM), the monomer fraction increases progressively while the triplet transient absorption remains low. Previous groups attributed this behavior to the reorganization of MB/SDS clusters as a prelude to the formation of normal micelles. During this stage, premicelles may be disaggregating with MB molecules released as MB/SDS quenched ion pairs.[7,36]

Finally, at SDS concentrations greater than 7 mM, the triplet transient absorption increases logarithmically until reaching a plateau corresponding to full monomerization. Concurrently, the absorption maximum at 665 nm is blue-shifted compared to the monomer spectrum signifying that the monomers are surrounded by a more polar environment than in water without SDS (most likely the negatively charged surface of the micelle) [Fig. 7(d)]. Therefore, the increase in monomer fraction can be explained by the increase of available sites for MB molecules to bind as the number of micelles increases.

In conclusion, an SDS concentration of 4 mM effectively promotes MB polymerization by playing a crossbinding role between the dye molecules. The large extent of polymerization (more than 95% of the initial monomers were transformed) makes this system a valuable tool for modeling the activation of a cleavable probe by photoacoustic contrast imaging.

3.3 *PLCI Imaging Between MB Monomers and Dimers in SDS*

Two plastic tubes, respectively containing 200 μM MB + 4 mM SDS (top) and 200 μM MB (bottom) solutions, were scanned by the PLCI system [Fig. 8(a)]. We estimated that the samples contained 5 and 110 μM monomer concentrations, respectively. For

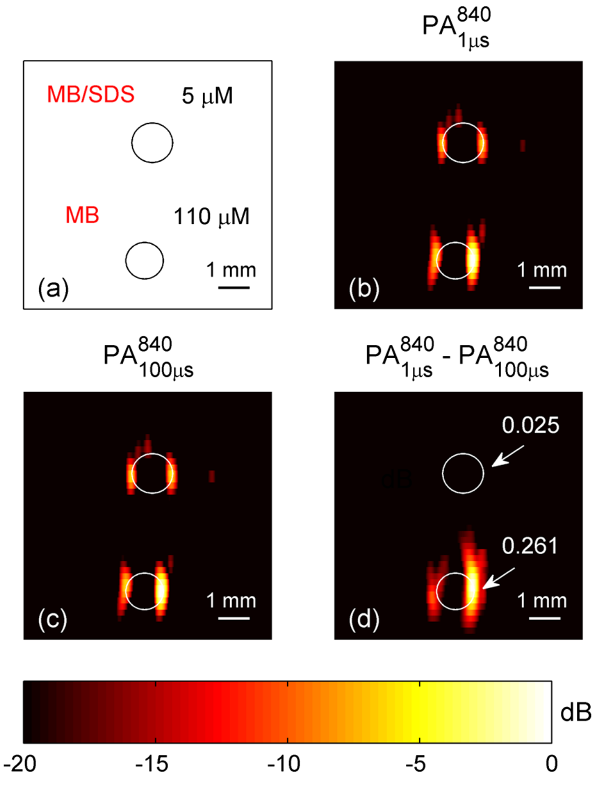

Fig. 8 (a) Schematic representation of the position and size of the plastic tubes. Monomer concentrations are given in each case. (b) Photoacoustic amplitude image at 840 nm recorded 1 μs after the excitation pulse shows the signal generated at the plastic wall–solution interfaces. (b) Photoacoustic amplitude image at 840 nm recorded 100 μs after the excitation pulse. (d) Difference between photoacoustic amplitude images at 1 and 100 μs. There is a 21.5 dB suppression of the background signal due to the short lifetime of MB dimers. The numbers represent the value of the contrast parameter C_{PLCI} at the front wall of the tubes.

this estimation, we first determined the monomer concentration in absence of SDS by applying the methodology described in 2.4 to the absorption spectrum of the MB-only sample. Because the addition of SDS induces the formation of a nonnegligible amount of trimers, we cannot use Eq. (6) to evaluate the monomer concentration of the second sample from the absorption spectrum. Alternatively, we determined this concentration by multiplying the monomer concentration in the absence of SDS by a proportionality factor corresponding to the difference in transient absorption between the two samples obtained by flash photolysis.

The samples were probed by a 10 MHz ultrasound transducer scanned perpendicularly to the tube axis within a range of 8 mm and with step size 0.2 mm. The signals were averaged over 32 measurements to compensate for pulse-by-pulse energy variations. The scanning time was relatively short (40 min) such that a majority of dimers (90%) remained stable during the experiment. At each step, we calculated the photoacoustic probe signal by subtracting the signal generated without the probe (excitation only) to the signal recorded with both beams (excitation + probe): $\mathrm{PA}_{840(t=\tau)} = (\mathrm{PA}_{660+840} - \mathrm{PA}_{660})_{t=\tau}$. As ground state MB molecules do not absorb at the probe wavelength (840 nm),[32] the signals measured at 100 μs correspond to the photoacoustic energy generated by the static background. The difference between the signal at 1 μs and the signal at 100 μs was computed to suppress the contribution of the background signal. The signals were processed with a Wiener filter followed by a low-pass filter (Butterworth, 6th order, cut off frequency at 6 MHz). The envelope was detected by the Hilbert transform method.

Photoacoustic images corresponding to 1 μs ($\mathrm{PA}_{840(t=1\ \mu\mathrm{s})}$) and 100 μs ($\mathrm{PA}_{840(t=100\ \mu\mathrm{s})}$) are displayed in Fig. 8 on a 20 dB scale as well as their difference. The circles correspond to the location and size of the plastic tubes. Dimer and background signals are efficiently suppressed by −21.5 dB in the differential image with a noise level of −59 dB [Fig. 8(d)]. The contrast parameter, calculated for the front wall of each tube, decreases by an average factor of 10 for the MB/SDS solution. Although C_{PLCI} is no longer proportional to the monomer concentration, possibly due to significant scattering in the MB/SDS solution, these results indicate that PLCI efficiently detects the monomer signal in a phantom object.

4 Conclusion

Here, we present a new contrast mechanism for photoacoustic imaging based on the difference in excited-state lifetime between monomer and dimer forms of a chromophore. We have studied two model systems to demonstrate the sensitivity of the PLCI method to aggregation states of MB dye. The addition of salt (sodium sulfate) provides a simple and direct way to change the self-association constant of MB solution and, therefore, the equilibrium dimer-to-monomer ratio. We have shown that the PLCI signal depends linearly on the monomer concentration as measured by analysis of optical absorption spectra. A second model system makes use of a surfactant (SDS) to induce MB dimerization. After careful study of the system, an optimal SDS concentration was identified that results in maximal dimerization of MB. This concentration is lower than the CMC of SDS in aqueous solution which implies that MB–SDS aggregates form premicellar structures. The PLCI imaging experiment reveals a contrast of more than 20 dB between two samples of equal MB concentration, one containing free MB solution and the other containing SDS-MB for maximal MB dimerization.

Activatable smart probes have been developed as research tools for studying protein conformational dynamics,[38,39] for detecting nucleic acid hybridization,[9,40] and for sensing enzymatic activity of disease biomarkers.[41–44] Based on the previous measurements, we propose a new mechanism for an activatable photoacoustic probe. In its simplest form, the probe relies on a custom-made peptide linker bearing a specific enzymatic site and confining two MB molecules to a dimer configuration. This configuration results in an intact, quenched probe of short lifetime. Reaction with endogenous enzymes cleaves the linker and separates the probe into MB monomers. The PLCI system would be used to selectively detect the long-lifetime signal from activated probes (monomers) which would provide a map of both enzyme location and activity. The lack of other long-lifetime molecules in the body empowers the sensitivity of this approach. We believe that PLCI probes could be implemented to investigate the role of specific enzymes in disease initiation and progression in animal models and establish preclinical data for translational research. Ultimately, PLCI probes could be developed as an early diagnosis tool and to monitor treatment efficacy.

Acknowledgments

The author is grateful to C. Sheaff for his assistance in reading the manuscript. This project was supported by NIH grant 1R21CA135027-01A1.

References

1. Y. Zhang, H. Hong, and W. Cai, “Photoacoustic imaging,” in *Imaging: A Laboratory Manual*, R. Yuste, Ed., CSHL Press, Cold Spring Harbor, New York (2011).
2. A. H. Green et al., “*In vitro* testing of a protease-sensitive contrast agent for optoacoustic imaging,” *J. Biomed. Opt.* **15**(2), 021315 (2010).
3. J. Levi et al., “Design, synthesis, and imaging of an activatable photoacoustic probe,” *J. Am. Chem. Soc.* **132**(32), 11264–11269 (2010).
4. P.-C. Li et al., “*In vivo* photoacoustic molecular imaging with simultaneous multiple selective targeting using antibody-conjugated gold nanorods,” *Opt. Express* **16**(23), 18605–18615 (2008).
5. R. W. Redmond and J. N. Gamlin, “A compilation of singlet oxygen yields from biologically relevant molecules,” *Photochem. Photobiol.* **70**(4), 391–475 (1999).
6. M. González-Béjar et al., “Methylene blue encapsulation in cucurbit[7]uril: laser flash photolysis and near-IR luminescence studies of the interaction with oxygen,” *Langmuir* **25**(18), 10490–10494 (2009).
7. D. Severino et al., “Influence of negatively charged interfaces on the ground and excited state properties of methylene blue,” *Photochem. Photobiol.* **77**(5), 459–468 (2003).
8. C. R. Drake, D. C. Miller, and E. F. Jones, “Activatable optical probes for the detection of enzymes,” *Curr. Org. Synth.* **8**(4), 498–520 (2011).
9. S. Tyagi and F. R. Kramer, “Molecular beacons: probes that fluoresce upon hybridization,” *Nat. Biotechnol.* **14**(3), 303–308 (1996).
10. C.-H. Tung, “Fluorescent peptide probes for *in vivo* diagnostic imaging,” *Peptide Sci.* **76**(5), 391–403 (2004).
11. V. Ntziachristos et al., “Fluorescence molecular tomography resolves protease activity *in vivo*,” *Nat. Med.* **8**(7), 757–761 (2002).
12. M. Heijblom et al., “Visualizing breast cancer using the Twente photoacoustic mammoscope: what do we learn from twelve new patient measurements?,” *Opt. Express* **20**(11), 11582–11597 (2012).
13. A. Garcia-Uribe et al., “*In vivo* diagnosis of melanoma and nonmelanoma skin cancer using oblique incidence diffuse reflectance spectrometry,” *Cancer Res.* **72**(11), 2738–2745 (2012).
14. J. I. Clifton and J. B. Leikin, “Methylene blue,” *Am. J. Ther.* **10**(4), 289–291 (2003).

15. K. Orth et al., "Methylene blue mediated photodynamic therapy in experimental colorectal tumors in mice," *J. Photochem. Photobiol. B Biol.* **57**(2–3), 186–192 (2000).
16. A. R. Disanto and J. G. Wagner, "Pharmacokinetics of highly ionized drugs II: methylene blue—absorption, metabolism, and excretion in man and dog after oral administration," *J. Pharm. Sci.* **61**(7), 1086–1090 (1972).
17. C. Peter et al., "Pharmacokinetics and organ distribution of intravenous and oral methylene blue," *Eur. J. Clin. Pharmacol.* **56**(3), 247–250 (2000).
18. S. Ashkenazi, "Photoacoustic lifetime imaging of dissolved oxygen using methylene blue," *J. Biomed. Opt.* **15**(4), 040501 (2010).
19. O. Yazdani et al., "Thermodynamic study of the dimerization equilibrium of methylene blue, methylene green and thiazole orange at various surfactant concentrations and different ionic strengths and in mixed solvents by spectral titration and chemometric analysis," *Dyes Pigments* **92**(3), 1031–1041 (2012).
20. K. Patil, R. Pawar, and P. Talap, "Self-aggregation of methylene blue in aqueous medium and aqueous solutions of Bu4NBr and urea," *Phys. Chem. Chem. Phys.* **2**(19), 4313–4317 (2000).
21. T. Förster, "Energy migration and fluorescence," *J. Biomed. Opt.* **17**(1), 011002 (2012).
22. M. Kasha, "Energy transfer mechanisms and the molecular exciton model for molecular aggregates," *Radiat. Res.* **20**(1), 55–71 (1963).
23. M. Kasha, H. R. Rawls, and M. Ashraf El-Bayoumi, "The exciton model in molecular spectroscopy," *Pure Appl. Chem.* **11**(3–4), 371–392 (1965).
24. A. Weller, "Electron-transfer and complex formation in the excited state," *Pure Appl. Chem.* **16**(1), 115–124 (1968).
25. S. Doose, H. Neuweiler, and M. Sauer, "Fluorescence quenching by photoinduced electron transfer: a reporter for conformational dynamics of macromolecules," *ChemPhysChem* **10**(9–10), 1389–1398 (2009).
26. R. M. Danziger, K. H. Bar-Eli, and K. Weiss, "The laser photolysis of methylene blue," *J. Phys. Chem.* **71**(8), 2633–2640 (1967).
27. H. C. Junqueira et al., "Modulation of methylene blue photochemical properties based on adsorption at aqueous micelle interfaces," *Phys. Chem. Chem. Phys.* **4**(11), 2320–2328 (2002).
28. K. J. Willis et al., "Fluorescence decay kinetics of the tryptophyl residues of myoglobin: effect of heme ligation and evidence for discrete lifetime components," *Biochemistry* **29**(22), 5270–5275 (1990).
29. E. Dimitrow et al., "Spectral fluorescence lifetime detection and selective melanin imaging by multiphoton laser tomography for melanoma diagnosis," *Exp. Dermatol.* **18**(6), 509–515 (2009).
30. A. van Hoek, J. Vervoort, and A. J. W. G. Visser, "A subnanosecond resolving spectrofluorimeter for the analysis of protein fluorescence kinetics," *J. Biochem. Biophys. Meth.* **7**(3), 243–254 (1983).
31. J. M. Beechem and L. Brand, "Time-resolved fluorescence of proteins," *Annu. Rev. Biochem.* **54**, 43–71 (1985).
32. R. S. Sonawane, S. G. Hegde, and M. K. Dongare, "Preparation of titanium(IV) oxide thin film photocatalyst by sol–gel dip coating," *Mater. Chem. Phys.* **77**(3), 744–750 (2003).
33. J. Cenens and R. A. Schoonheydt, "Visible spectroscopy of methylene blue on hectorite, laponite B and barasym in aqueous suspension," *Clay Clay Miner.* **36**(3), 214–224 (1988).
34. E. Rabinowitch and L. F. Epstein, "Polymerization of dyestuffs in solution. Thionine and methylene blue," *J. Am. Chem. Soc.* **63**(1), 69–78 (1941).
35. E. Touitou and P. Fisher, "Prevention of molecular self-association by sodium salicylate: effect on methylene blue," *J. Pharmaceut. Sci.* **75**(4), 384–386 (1986).
36. M. K. Carroll et al., "Interactions between methylene blue and sodium dodecyl sulfate in aqueous solution studied by molecular spectroscopy," *Appl. Spectrosc.* **53**(7), 780–784 (1999).
37. X. Liu, X. Wu, and J. Yang, "Protein determination using methylene blue in a synchronous fluorescence technique," *Talanta* **81**(3), 760–765 (2010).
38. J. Zhang et al., "Genetically encoded reporters of protein kinase A activity reveal impact of substrate tethering," *Proc. Natl. Acad. Sci. U. S. A.* **98**(26), 14997–15002 (2001).
39. S. Liu, J. Zhang, and Y. K. Xiang, "FRET-based direct detection of dynamic protein kinase A activity on the sarcoplasmic reticulum in cardiomyocytes," *Biochem. Biophys. Res. Commun.* **404**(2), 581–586 (2011).
40. V. V. Didenko, "DNA probes using fluorescence resonance energy transfer (FRET): designs and applications," *Biotechniques* **31**(5), 1106–1121 (2001).
41. R. Weissleder et al., "*In vivo* imaging of tumors with protease-activated near-infrared fluorescent probes," *Nat. Biotechnol.* **17**(4), 375–378 (1999).
42. T. Jiang et al., "Tumor imaging by means of proteolytic activation of cell-penetrating peptides," *Proc. Natl. Acad. Sci. U. S. A.* **101**(51), 17867–17872 (2004).
43. J. H. Ryu et al., "Optimization of matrix metalloproteinase fluorogenic probes for osteoarthritis imaging," *Amino Acids* **41**(5), 1113–1122 (2011).
44. J. Levi et al., "Molecular photoacoustic imaging of follicular thyroid carcinoma," *Clin. Cancer Res.* **19**(6), 1492–1502 (2013).